Materials Chemistry and Physics 277 (2022) 125264

Contents lists available at ScienceDirect

Materials Chemistry and Physics

journal homepage: www.elsevier.com/locate/matchemphys

Controlled synthesis of luminescent ZnS nanosheets with high piezoelectric performance for designing mechanical energy harvesting device

Siju Mishra [a], P. Supraja [a], P.Ravi Sankar [b], R.Rakesh Kumar [a], K. Prakash [b], D. Haranath [a,*]

[a] Energy Materials and Devices Laboratory, Department of Physics, National Institute of Technology, Warangal, 506 004, India
[b] Flexible Electronics Laboratory, Department of Electronics and Communication Engineering, National Institute of Technology, Warangal, 506 004, India

HIGHLIGHTS

- Cubic ZnS nanosheets were made using a low-temperature hydrothermal technique.
- When finger tapped, our nanogenerator produced an open-circuit voltage of ~400 mV.
- When toe pressed, our nanogenerator produced an open-circuit voltage of ~600 mV.
- By connecting series of nanogenerators, the output voltage increased tremendously.
- The stability of nanogenerator was unique when observed at various time intervals.

GRAPHICAL ABSTRACT

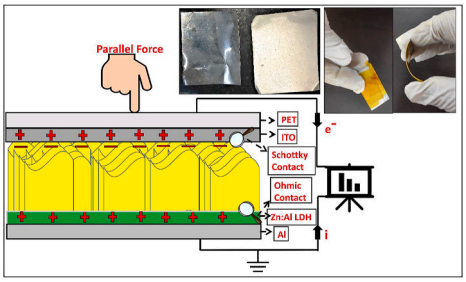

ARTICLE INFO

Keywords:
Hydrothermal method
Zinc sulfide nanosheet
Piezoelectric
Photoluminescence
Nanogenerator device

ABSTRACT

For the first time, single-step fabrication of two-dimensional nanosheets of zinc sulfide (ZnS) was achieved employing flexible aluminum (Al) foil substrate using hydrothermal technique at 140 °C for ~4 h. Indium doped Tin Oxide (ITO) coated on PET (Polyethylene Terephthalate) substrate and ZnS deposited Al foil as a top and bottom electrodes were used to fabricate a piezoelectric device. To generate an electric potential, the top ITO electrode was tapped on the ZnS nanosheets. The open-circuit voltage, V_{OC} of ~400 mV was obtained and analyzed for ZnS nanosheets based nanogenerator with gentle finger taping. However, the highest output for the single nanogenerator was found to be ~600 mV by applying toe pressure. Additionally, switching polarity and superposition experiments were utilized to confirm the nanogenerator's performance, with the findings confirming piezo-electric voltage output. This study investigates the new potential for a ZnS-based high-efficient energy harvester that can scavenge biomechanical energy for next-generation flexible self-powered electronics devices as well as a good replacement for ZnO nanosheets in 2D nanostructured based nanogenerator devices due to its simple single-step production process, low cost, and high output gain.

1. Introduction

Renewable energy sources have been the attention of researchers in recent decades as a means of replacing fossil fuels such as coal, crude oil, and natural gas etc. The rapid development of transparent flexible electronics holds a lot of potential for next-generation energy devices for

* Corresponding author.
E-mail address: haranath@nitw.ac.in (D. Haranath).

https://doi.org/10.1016/j.matchemphys.2021.125264
Received 29 July 2021; Received in revised form 13 September 2021; Accepted 16 September 2021
Available online 13 October 2021

self-powered nanosystems and nanosensors. Because of their potential to generate electricity from biomechanical motions, vibrations, heat, human motion, and auditory energies, piezoelectric nanogenerators have attracted a lot of attention [1–4]. The piezoelectric effect was discovered by Curie in 1880, but it was not exploited in a practical application until 2006 when piezoelectric capabilities based on ZnO nanogenerators were discovered [5]. Researchers have recently been working on self-powered nanodevices and sensors that are powered by nanogenerators [1]. One-dimensional (1D) environmental-friendly lead-free piezoelectric materials nanostructures have gotten a lot of interest because of their non-toxic nature and great optical, electrical, semiconducting, and piezoelectric properties. These characteristics allowed them to be used in a wide range of applications, including electronics, optoelectronics, electromechanical, and electrochemical systems [6–12]. Now growth of nanorod, on the other hand, is a multistep process that often requires additional seed layer coating and annealing at a higher temperature [13]. As time goes on, this multistep growth mechanism gets more intricate and costly. However, due to properties such as nanometer-scale thickness, a high surface-to-volume ratio, and superior mechanical stability, two-dimensional (2D) ZnO nanostructures, such as nanowalls [14], nanoplatelets [15] and nanosheets [16,17] are becoming more popular to overcome this lengthy procedure [18,19]. Nanosheets can be produced using a variety of techniques, including the solvothermal process [20], microwave-assisted synthesis [21], thermal evaporation [22], hydrothermal synthesis [23], carbothermal reduction [24], and electrodeposition [25]. The hydrothermal solution-assisted growth strategy is the most suitable for 2D nanostructures [26] because of the flexibility to perform the synthesis process on a range of substrates at low temperatures, uniform growth on large surfaces, relatively easy synthesis procedures, cost-effective, less poisonous, and environmentally friendly.

Piezoelectric nanogenerators (PENG) have a sandwich structure i.e. the piezoelectric materials merged between two electrodes [14]. Due to deformation in crystal symmetry, the piezoelectric potential is produced between the electrodes when mechanical force is applied at the top ITO electrode or while stretching the device. The negative charges are separated from the top electrode by the piezoelectric potential created by piezoelectric materials such as ZnO and GaN. The charges return to their original condition when mechanical stress is removed [27,28]. Several reports on piezoelectric nanogenerator fabrication using nanostructures of ZnO, $BaTiO_2$, $PbTiO_3$, GaN, InN, PZT, PVDF [29–34]. The existing literature on piezoelectric nanogenerators has several disadvantages: (1) high-temperature synthesis for nanostructures formation [29–32], (2) nanogenerator fabrication process with other piezoelectric material is a multi-step process [31], [34], (3) some piezoelectric materials are toxic and not bio compatible [29], [33], (4) preparation methods are expensive for other piezoelectric materials [29–32].

In the current manuscript, ZnS nanosheet-based nanogenerator is explored for the first time. To the best of our knowledge, only four reports are dealing with the piezoelectric nanogenerators fabrication using ZnS nanorods [35,36], ZnO–ZnS [37], and another one ZnS- PANI/PVDF [38]. ZnS is the most promising material with a direct bandgap of 3.54 eV and having piezoelectric and semiconducting capabilities. The current study with ZnS has several advantages compare to reported piezoelectric nanogenerators with other materials. The first advantage is the cost-effective and low-temperature hydrothermal synthesis of ZnS nanostructures. The second advantage is single-step device fabrication as no additional electrode deposition is required. The third advantage is ZnS nanostructures growth on a large-area substrate is easy, and it helps scale the production. In addition to the above, ZnS has excellent acoustoelectric properties and optical conductivity and thus can be used in diverse applications [39].

For the first time, we present a nanogenerator made up of a 2D ZnS nanosheets network developed at 140 °C utilizing a single-step modified hydrothermal technique as mentioned in our previous report with no seed layer deposition [40]. After synthesis, excellent and consistent piezoelectric output voltages of ~400 mV were obtained from a single device with gentle finger tapping. Also, we worked on new technologies that harvest energy from vibrations or disturbances induced by footsteps, heartbeats, ambient noise, and airflow that operate at low frequencies (such as ≤10 Hz) and are based on flexible soft materials are critical to evaluate [41]. Here we present a simple, low-cost approach for turning low-frequency vibration/friction energy into electricity using a 2D cubic-ZnS piezoelectric nanogenerator. A piezoelectric potential can be produced in any bulk or nanostructured semiconductor crystal having non-central symmetry, such as the Group III–V and II-VI materials, due to the polarization of ions under applied stress and strain conditions. This property is common to both zinc blende and wurtzite crystal structures. From structural point of view, both wurtzite and zinc blende structures are non-centrosymmetric and thereby possess piezoelectric property. Scheme-1 shows the pictorial representation of zinc blende structured ZnS under normal and strain conditions, respectively. However, there is only one independent piezoelectric coefficient in zinc blende, called e14, coupled to shear components of the strain [42], whereas, in wurtzite, there are three independent piezoelectric coefficients: e31, e33, and e15. Here, we report for the first time, zinc blende structured ZnS for nanogenerator applications. We measured the I–V characteristics of the as-fabricated nanogenerator were Schottky like, and it produced harvesting currents constructively [28]. The detailed methodology, material analysis, optical and electrical studies are discussed in the later sections.

2. Experimental

Zinc chloride anhydrous ($ZnCl_2$, 99%, FINAR) for Zinc source, thiourea (NH_2CSNH_2, 99% FINAR) for sulfur source, ethylenediamine ($C_2H_4(NH_2)$, 99.5% SRL) as a structure directing coordination molecular template and deionized (DI) water were used to grow the ZnS nanostructures [35]. The aluminium foil of thickness 0.1 mm is used as substrate. The hydrothermal (or solvothermal) approach is a good way to make two-dimensional nanostructures like nanosheets, nanoflakes, nanowalls, and so on [20,23]. Here, in this study, we followed a modified single-step hydrothermal method to develop ZnS nanosheets [40]. Before the synthesis of ZnS nanosheets, the Al substrate was cleaned with acetone, DI water, and ultrasonicated for about 10 min. After that ZnS nanosheet growth solution was prepared, using $ZnCl_2$ and thiourea in 1:3 M ratio, mixed well with 100 mL aqueous solution of ethylenediamine (EN) (1:1) under continuous magnetic stirring for 20 min, as shown in Scheme 2. Then the Al substrate was placed over the solution very slowly so that because of the surface tension, the cleaned aluminium substrate should float on top of the growth solution. Now for the bottom electrode, kapton tape was used to cover a small area of each substrate. The growth solution and substrates were sealed in a glass beaker with aluminium foil and put in a hot air oven for about 4 h at 140 °C. The substrates were allowed to cool to room temperature after the growth process. The substrates were then removed and thoroughly washed with DI water to remove organic salts before drying at room temperature. After that, a light white-coloured nanostructured film was observed over the Al substrate. Bending, twisting, and rolling is also possible with this synthesized ZnS film on Al substrate.

3. Fabrication of nanogenerator

Leaving space for electrode contacts, the nanogenerator was prepared and sealed with kapton tape, by installing the ITO-coated PET substrate on the ZnS nanosheets' surface without any short circuit. Two connecting cables were used to connect the ITO-PET substrate and the aluminum substrate. To record the produced open-circuit voltage, the Digital Oscilloscope (Tektronix TBS-1102) was connected to a computer through connecting software (Tek-VISA) as shown in Scheme 3. The synthesized ZnS 2D nanosheets are characterized by X-ray diffraction analysis, scanning electron microscope. The inset of Scheme 3,

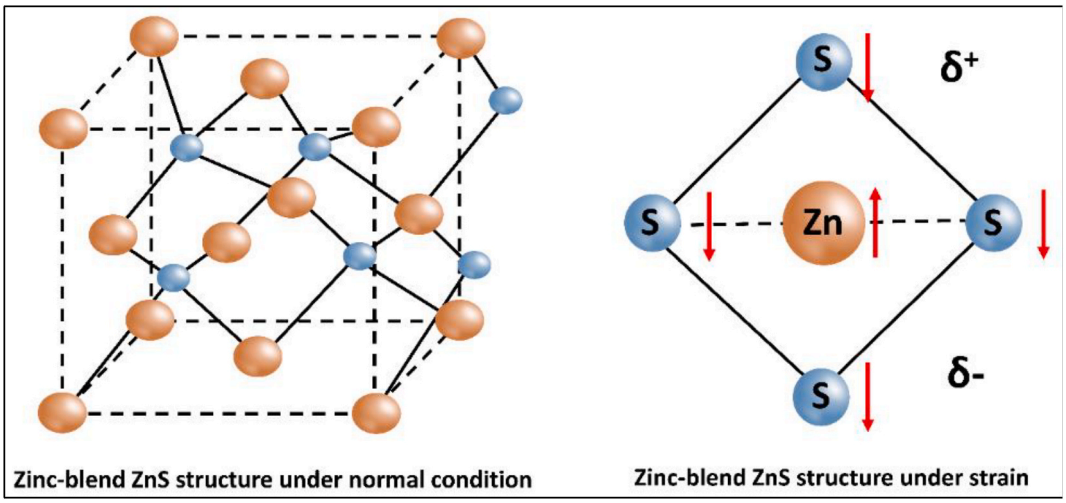

Scheme 1. Pictorial representation of zinc blende structured ZnS under normal and strain conditions.

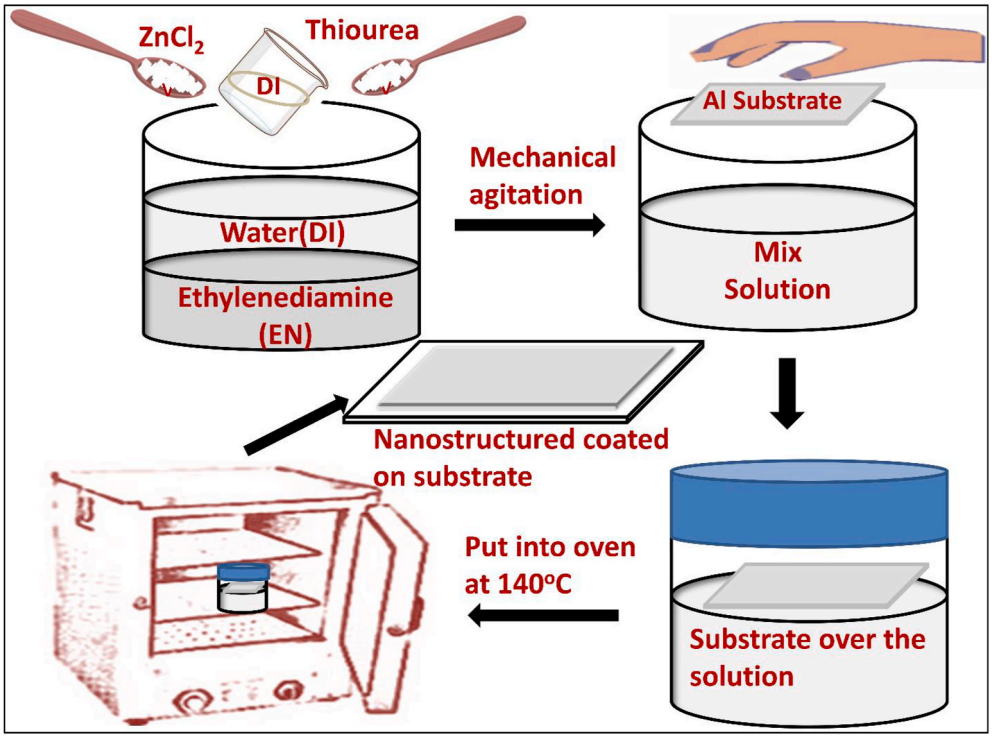

Scheme 2. Synthesis process of ZnS nanosheets.

represents the real-time image of coated ZnS on Al foil as well as fabricated ZnS PENG with normal and bending conditions. The electrical characterization of nanogenerator also done with DSO (Digital storage oscilloscope, Tektronix-TBS1102) and optical properties of collected powder from the solution measured by using photoluminescence (PL) and UV-VIS spectroscopy technique.

4. Results and discussion

4.1. Surface morphology analysis by FE-SEM

The field emission scanning electron microscopy (FE-SEM, Zesis merlin) technique was used to monitor the morphology of grown ZnS nanostructures at various magnifications. Fig. 1(a and b) portrays the obtained ZnS nanosheets which are evenly distributed throughout the substrate. Nanosheets that are dense and porous can be seen all over the substrate. Fig. 1(c) shows the EDAX spectrum obtained on ZnS nanosheets. It confirms the purity of ZnS nanosheets by revealing the presence of Zn, S, and Al.

4.2. Crystalline analysis by X-ray diffraction (XRD)

Fig. 1(d) shows the X-ray diffraction (XRD, X-pert Pro-PW 3050/50) pattern of ZnS nanosheets on Al substrate. The XRD pattern obtained is well-matched and indexed with the standard (JCPDS card-80-0020) [43]. The diffraction peaks at 28.64°, 47.16°, 56.03° correspond to (111), (022), (131) planes of the cubic ZnS which confirm the crystalline nature of ZnS. Most of the diffraction peaks had broad full width at half maximum (FWHM) values, indicating the production of crystallites with small dimensions. The Debye-Scherrer formula is used to compute the

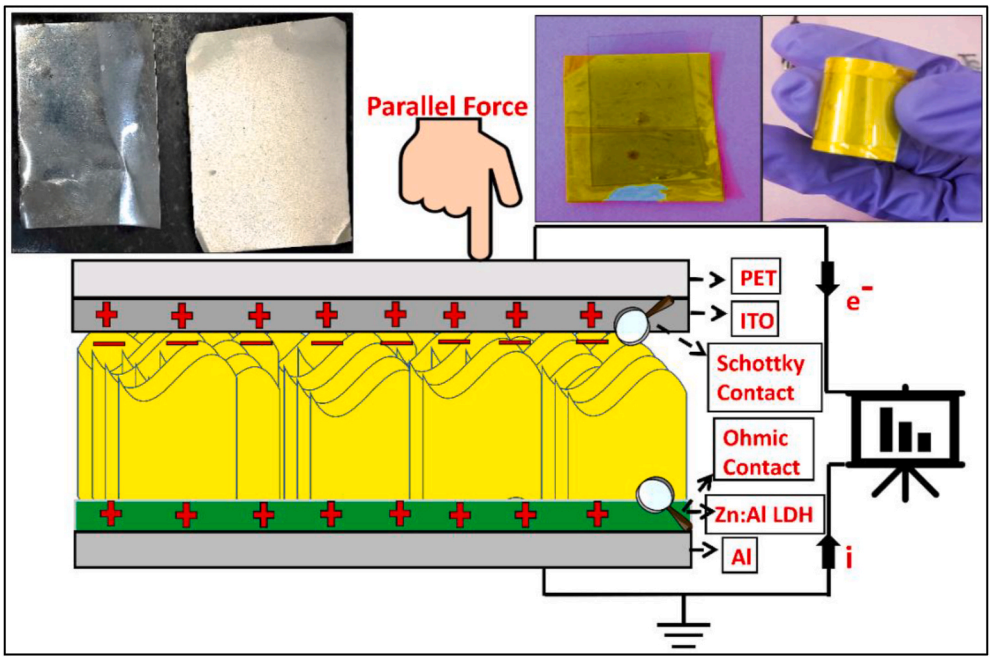

Scheme 3. Cross-sectional view of the fabricated device. Inset shows an optical image of the device.

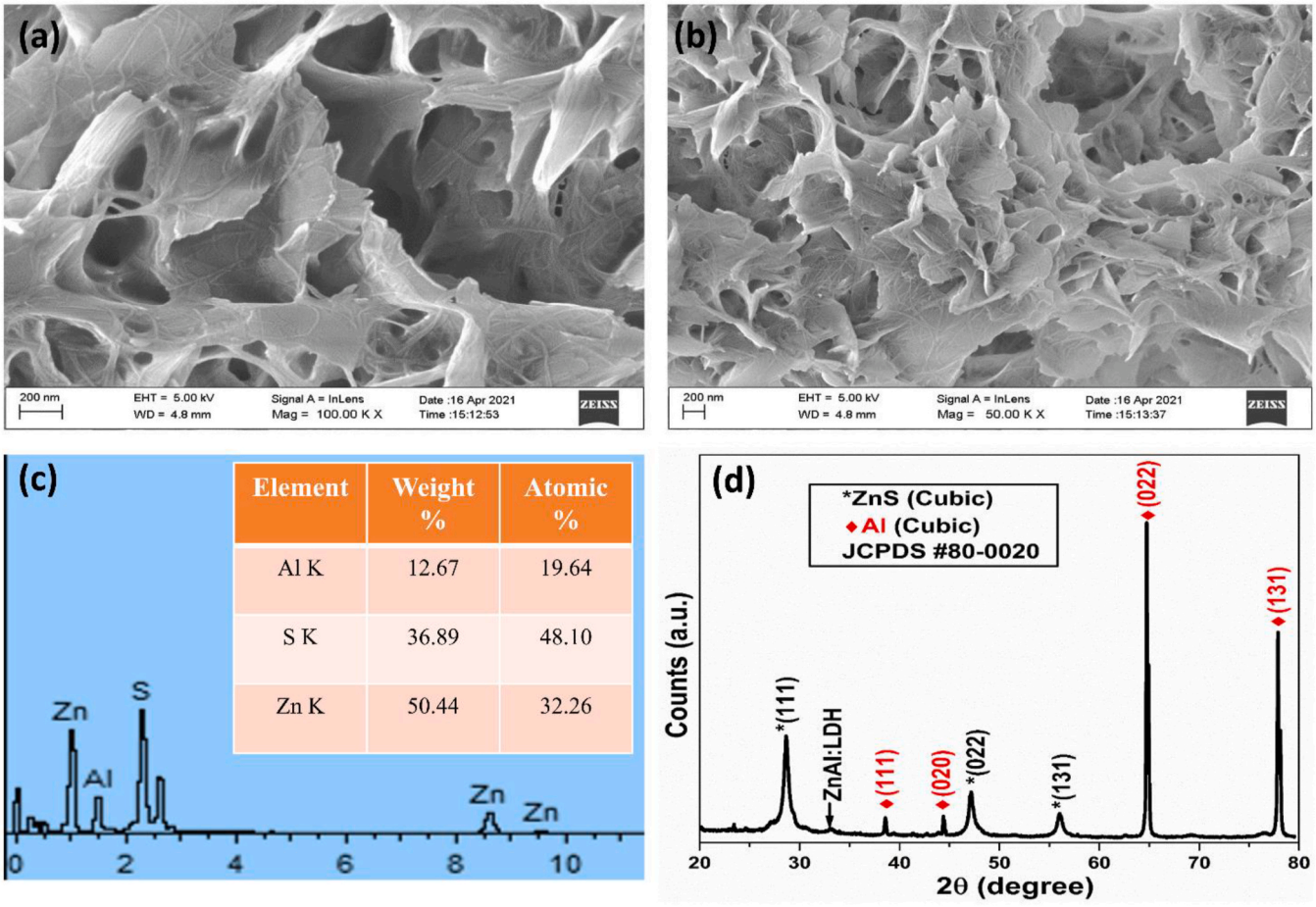

Fig. 1. (a, b) Surface morphology of ZnS nanostructure for different magnifications, **(c)** EDAX analysis, **(d)** XRD of ZnS nanostructure with the substrate.

grain size of crystalline ZnS. The average grain size derived by considering the three most intense ZnS diffraction peaks is roughly 16.16 nm. The intense diffraction peaks at 38.58°, 44.38°, 64.75°, 77.87° corresponds to (111), (020), (022), (131) plane of cubic aluminium (JCPDS card-85-1327) coming directly from the substrate. The additional diffraction peaks at 33.06° and the corresponding plan (012) also confirm the formation of ZnAl: LDH at the interface of ZnS nanostructures and aluminium [40,44].

4.3. Optical studies using photoluminescence (PL) and UV-VIS spectra

Photoluminescence (PL) studies, in general, provide details about defect states that contribute to the sample's de-excitation through radiation. According to PL investigations, the defect states in nanocrystals can vary or the density can increase. Fig. 2(a) shows the PL emission (463 nm) and excitation (393 nm) spectra of ZnS powder sample. The ZnS powder was collected from the glass beaker by filtration and the PL spectra were recorded at room temperature (25 °C) using Horiba Jobin Yvon Flurolog FL3-21 spectrofluorometer. This study indicates that impurities or surface states play a significant role in the PL phenomenon. The energy level diagram in Fig. 2(b) can be used to deduce the luminescence mechanism. Surface states, such as Zn^{2+} or S^{2-} ions, generate energy states inside the bandgap in nanocrystals. Electrons in the valence band (VB) or Zn^{2+} levels are excited by higher-energy photons (393 nm), allowing them to travel into the conduction band (CB). Non-radiative decay of excited electrons to surface states before radiatively decaying to the valence band and releasing lower-energy photons. The valence band edge moves downwards as particle size decreases. As a result, the emitted photons have more energy and produce photoluminescence at a shorter wavelength [40,45]. Further, new studies have been explored in the literature on the conversion of mechanical energy to optical energy, and it opens up a new window for research [46,47].

The absorption spectra of ZnS powder is shown in Fig. 2(c). The UV-VIS spectrum is normally affected by the size of the nanocrystals, and the maximum wavelength of absorption decreases with particle size. As compared to bulk phase ZnS (340 nm), the peaks have been blue-shifted (235 nm). This change in absorption is primarily due to quantum confinement effects, which reveals the shift in the bandgap [48,49]. The calculated band gap of the ZnS nanopowder was 3.83 eV also shown in Fig. 2(d).

4.4. Characteristics of nanogenerator

Heat and kinetic energy from physical movement make up tremendous amounts of energy in the human body. This creates interest for effectively utilizing this enormous power. With the advancement of low-power gadgets, it is now possible to use the human as a self-powered system to power wearable electronic equipment. Here, we show energy harvesting from human body movement using a ZnS NSs nanogenerator to transform biomechanical energy to electrical energy. The nanogenerator was effectively strained by using body movements such as wrist folding, toe pressure, and finger pressing and stretching. The output of the nanogenerator was tested under periodic bending and

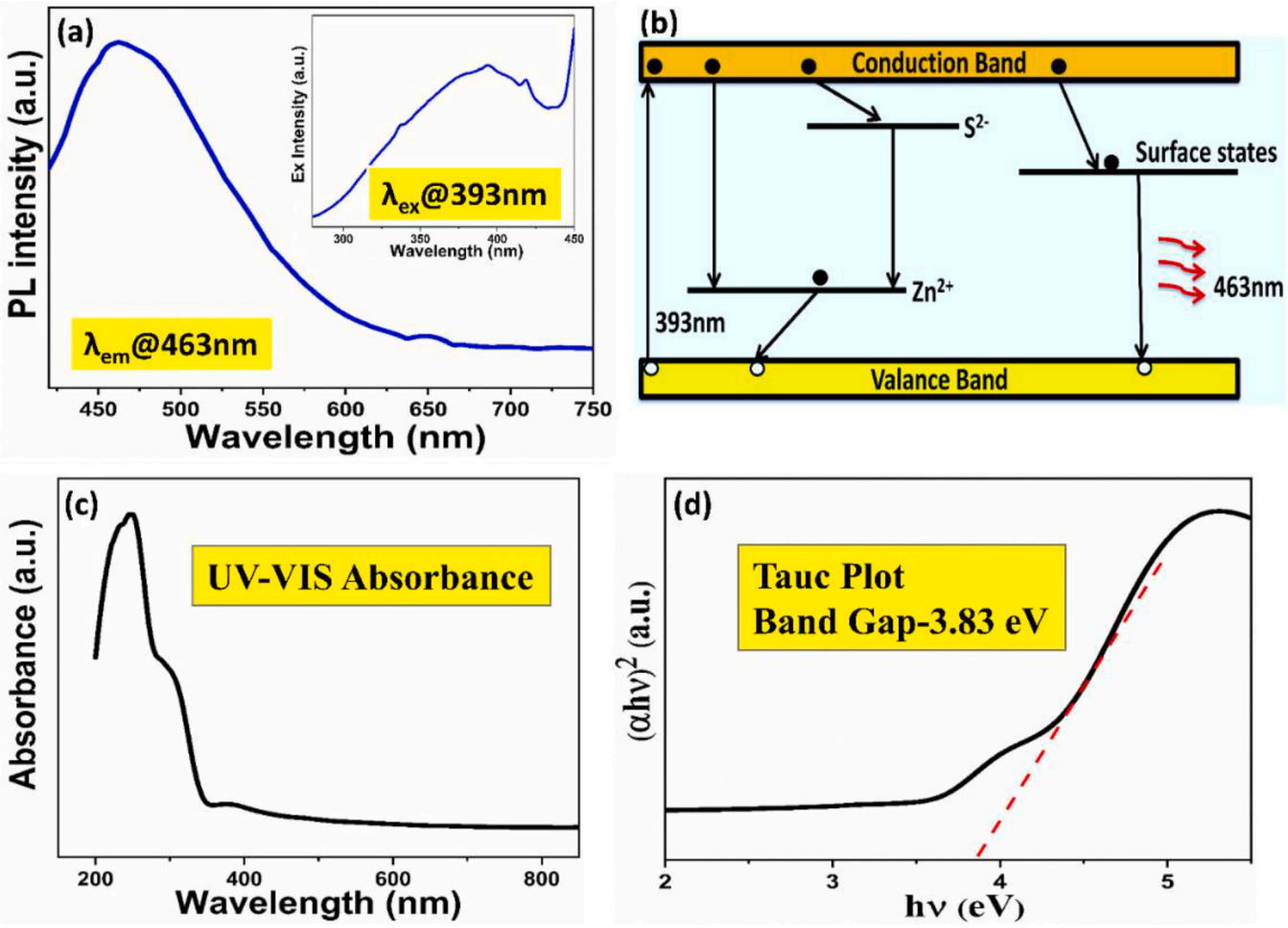

Fig. 2. (a) The PL spectrum of ZnS nanopowder excited at 393 nm. Inset shows the excitation spectrum, **(b)** The energy band diagram of ZnS nanopowder, **(c)** Absorption spectra of ZnS nanopowder, **(d)** Bandgap estimation from the Tauc plot.

unbending circumstances. The manufactured nanogenerator device response was also checked for different sources of pressure like impact with punch, stick, toe pressure to harvest energy.

The finger tapping with moderate pressure (active area 2 × 3 cm^2) was mainly used, to determine the piezoelectric efficiency of fabricated ZnS-based nanogenerator as well as a different type of characteristics. The open-circuit voltage was measured by using a Tektronix-TBS1102 digital oscilloscope connected to a monitor. As we apply force to the nanogenerator, the resulting stress distorts the symmetry of the ZnS lattice and causes a dipole to form. The potential is formed in the system because of the non-net zero dipole moment (Fig. 3(a)). Because of the non-equilibrium in the charge center, the electron will drive through the surface of the top electrode to the bottom electrode, resulting in a positive potential peak in the measurement. When the device's external tension is removed, the dipole moment gets vanished [28]. The electron flow is mainly controlled by the Schottky barrier forms between the ZnS and ITO electrode interfaces due to different work function [50,51]. The power generation mechanism is very well explained in the previous literature [37,52]. Now the nanogenerators' responses to repetitive finger tapping in both the forward and reverse directions are shown in Fig. 3(b). Each finger tapping produces an output voltage of 350–400 mV. When compared to the literature reports, the current NG giving higher output than ZnO [53], MoS_2 [54], Wse_2 [55], and ZnO–ZnS based nanogenerators [56]. Further, the current NG output is less than the ZnS nanorod, ZnS fiber-based nanogenerators. Details of the piezoelectric nanogenerator fabricated with different materials and performance depocted in the literature has been presented as Table S1 of Supplementary Information.

To determine whether the created voltage is related to piezoelectric effect or other artefacts such as instrumentation noise, switching polarity tests and voltage superposition tests were performed. When the polarity is swapped, the output response is measured by reversing the connections, and the output voltage for each tapping finger is displayed in Fig. 3(b). For reverse connections, the output voltage is the exact inverse of that produced for forward connections. The output voltage was created by the nanogenerator device itself rather than instrument noise, revealed by the switching polarity test [19,57]. Any noise signal created by the measuring device will not shift its sign from positive to negative when the connections are reversed. By connecting two devices in series, the voltage superposition test was also performed to evaluate the measured output voltage. The sum of the individual nanogenerators voltages will be equal to the output voltage. A forward connection of two nanogenerators in series results in an output voltage of 750–800 mV (Fig. 3(c)).

The variation of electrical outputs under various external loads ranging from 30 kΩ to 70 MΩ is monitored under constant finger tapping pressures. Fig. 3(d) depicts the change in average output voltage under various external load resistances. Along with the increase in load resistance, the output voltage also rose. At larger load resistances of 50 MΩ and above, the output voltage reaches saturation. According to the literature, the saturated value of output voltage with increasing resistance is attributable to the open-circuit voltage [36,58]. The device's power is calculated using the formula $P = V^2/R_L$. Fig. 3(e) depicts the changing of the PENG's output power with the external load resistance. At a load resistance of 100 kΩ, the maximum output power of 219.5 nW is attained with an output voltage of ~148 mV. PENG is also tested for bending and twisting movements. The PENG's response to bending and twisting is depicted in Fig. 3(f). For bending and twisting movements of the device, output voltages exceeding 375 mV and 400 mV are found mainly due to the large area deformation of the ZnS nanosheets.

A long-term stability test was also carried out to ensure the PENG's

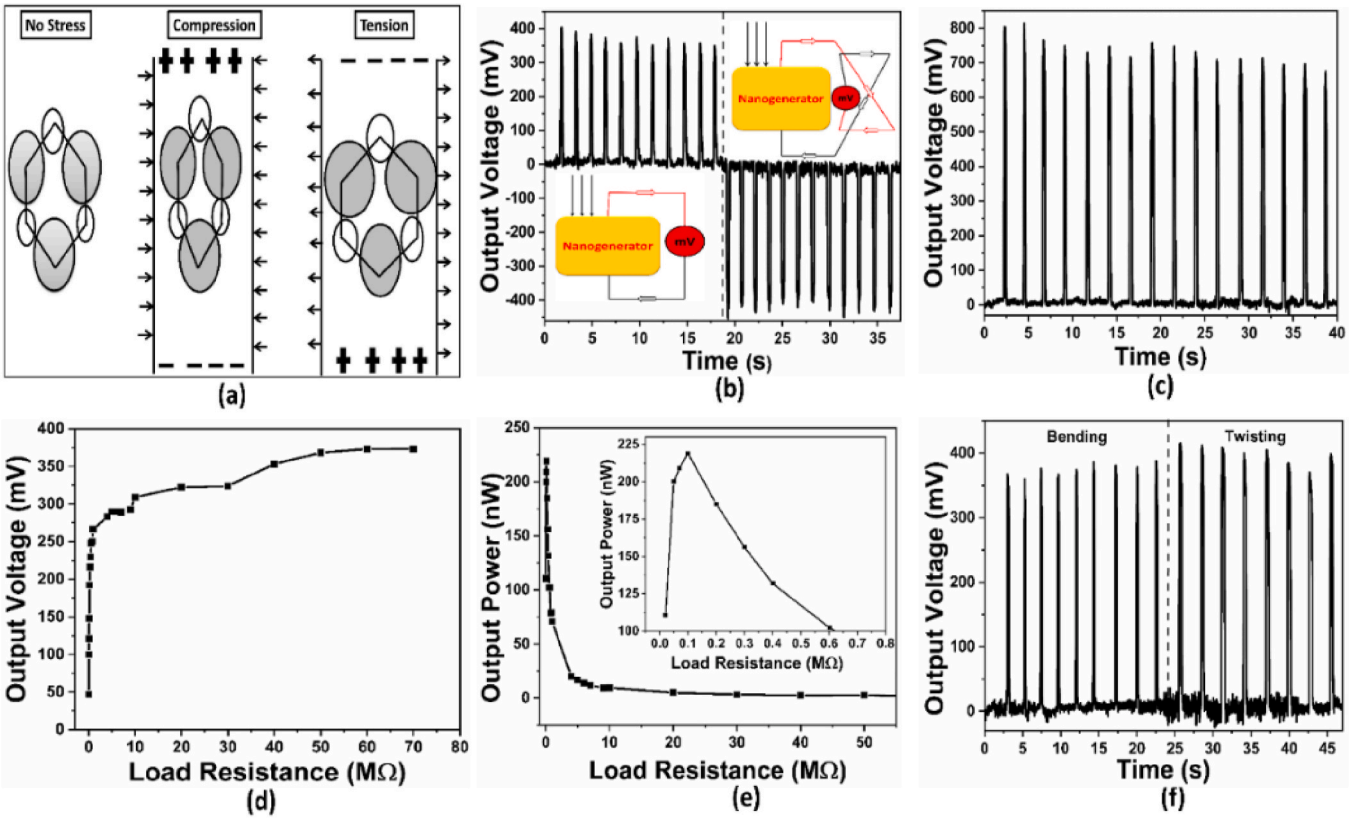

Fig. 3. (a) Schematic of piezoelectric generation, **(b)** Electric output of PENG under forward and reverse connections, **(c)** Output voltage of two devices in series under forwarding bias condition, **(d)** Output voltage with variable load resistance, **(e)** Instantaneous power output with variable load resistance (Inset is the enlarged version of maximum power around 219.5 nW), **(f)** Output response for Bending and Twisting the device.

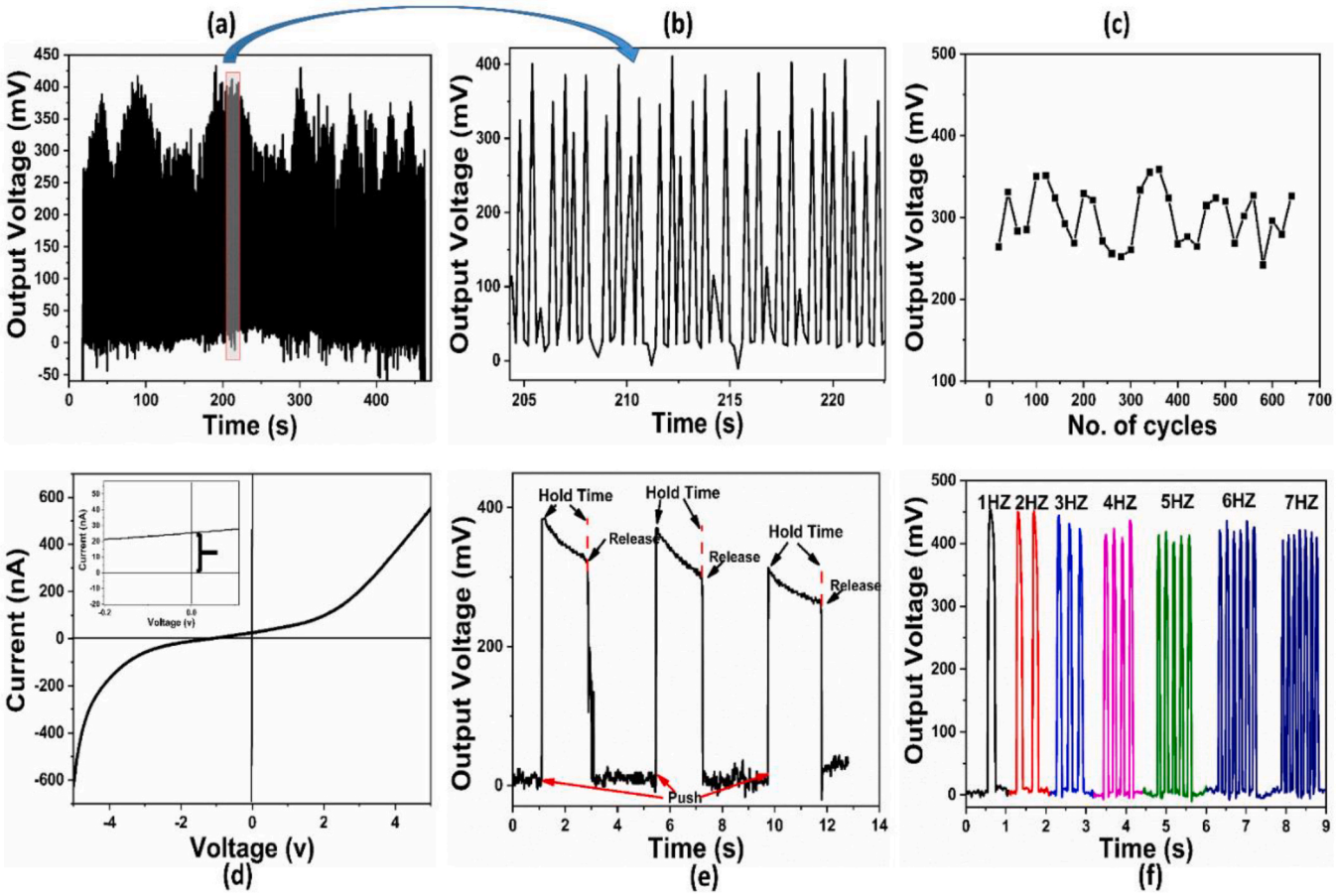

Fig. 4. (a) Long term stability test, **(b)** Enlarge image of the stability output, **(c)** Variation of Output Voltage after every 20 cycles **(d)** Schottky like I–V characteristics (inset image shows the non-zero current at origin), **(e)** Constant force applied on the device for a longer time, **(f)** Different frequency response.

mechanical stability and endurance. The response of the nanogenerator over 1260 cycles of repetitive finger tapping is shown in Fig. 4(a). Overall, of the cycles, the manufactured PENG has shown an approximately constant response. The tiny difference in output voltages after every 20 cycles from zero to 650 cycles is due to finger tapping pressure variations (Fig. 4(c)). After 1260 cycles, the generated output voltage from PENG does not significantly change. Fig. 4(d) shows the current-voltage characteristics (I–V) of the fabricated piezoelectric device. The nanogenerator also exhibited Schottky-like I–V characteristics between ITO and nanosheets as well as constructively generated harvesting currents due to the formation of non-ohmic barrier at the ITO and ZnS nanosheets junction [28]. Now, the I–V characteristics shown a minor non-zero current (~24 nA) for zero voltage at the origin. This is probably due to the photovoltaic effect or due to the dark current present in the nanogenerator (Inset of Fig. 4(d)). When the applied force is maintained at a constant level for an extended period, the piezo-potential steadily decreases (Fig. 4(e)). The positive piezo-potential produced by ZnS nanosheets attracts ITO electrode electrons, causing the piezo-potential to decrease. As long as the applied force remains constant, the voltage pulse will gradually decrease. In the absence of external force, the voltage pulse, on the other hand, did not perfectly return to its original state. This is because of the minimal piezo potential that remained throughout the holding time and could not be fully screened. After the removal of external force, the device output returns to its original state [40].

The frequency of the nanogenerator with applied pressure was also carried out (~7 Hz) for confirming the low-frequency response of this device shown in Fig. 4(f) which also demonstrates that the manufactured device can be used to successfully harvest lower frequency ranges of movements from human body motion and ambient mechanical sources [41].

To illustrate the nanogenerator's practical applicability, the generated power must be stored in an external device such as a capacitor, supercapacitor, or battery. We utilized a capacitor to hold the generated voltage and then used it to power a commercial red LED.

Capacitors were charged to get a direct idea of the manufactured ZnS PENG's energy production capability. The nanogenerator received mechanical energy from gentle human finger tapping (3 Hz), which was immediately used to charge up to four separate capacitors. During a periodic compression and release cycle, Fig. 5(a) shows the capacitors being steadily charged utilizing PENG generated power. The voltage across the 0.5 μF, 1 μF, 2.2 μF, 4.7 μF capacitors are 468 mV, 464 mV, 458 mV, 419 mV respectively within only 60 s. Within 15 s, the steady-state condition was achieved. Fig. 5(b, c, d) shows the accumulated charge (Q = CV) in each capacitor, maximum output voltage & maximum stored charge across the different capacitors, rate of energy-storing in each capacitor with time respectively. Based on the NG's charging capabilities, the stored energy in the capacitors is calculated using the equation $E_c = 1/2\ CV^2$. Hence by the results, we can say that 0.5 μF stored charge very quickly and also discharge quickly, whereas 4.7 μF charged to maximum value after a couple of seconds (~50 s) and also discharged very slowly. The numerical calculations ($f = 1/(2\pi RC)$), f = 3 Hz tapping frequency, (C = 0.5 μF) shows that the reactance of 0.5 μF capacitance is approximately 106.1 kΩ at 3 Hz. Regarding Fig. 3 (e) where maximum power was achieved at RL of 100 kΩ which is resembled to the reactance of CL at 0.5 μF [59]. It's worth mentioning that the PENG's high charging performance is achieved without the need for any external poling or triboelectric processes.

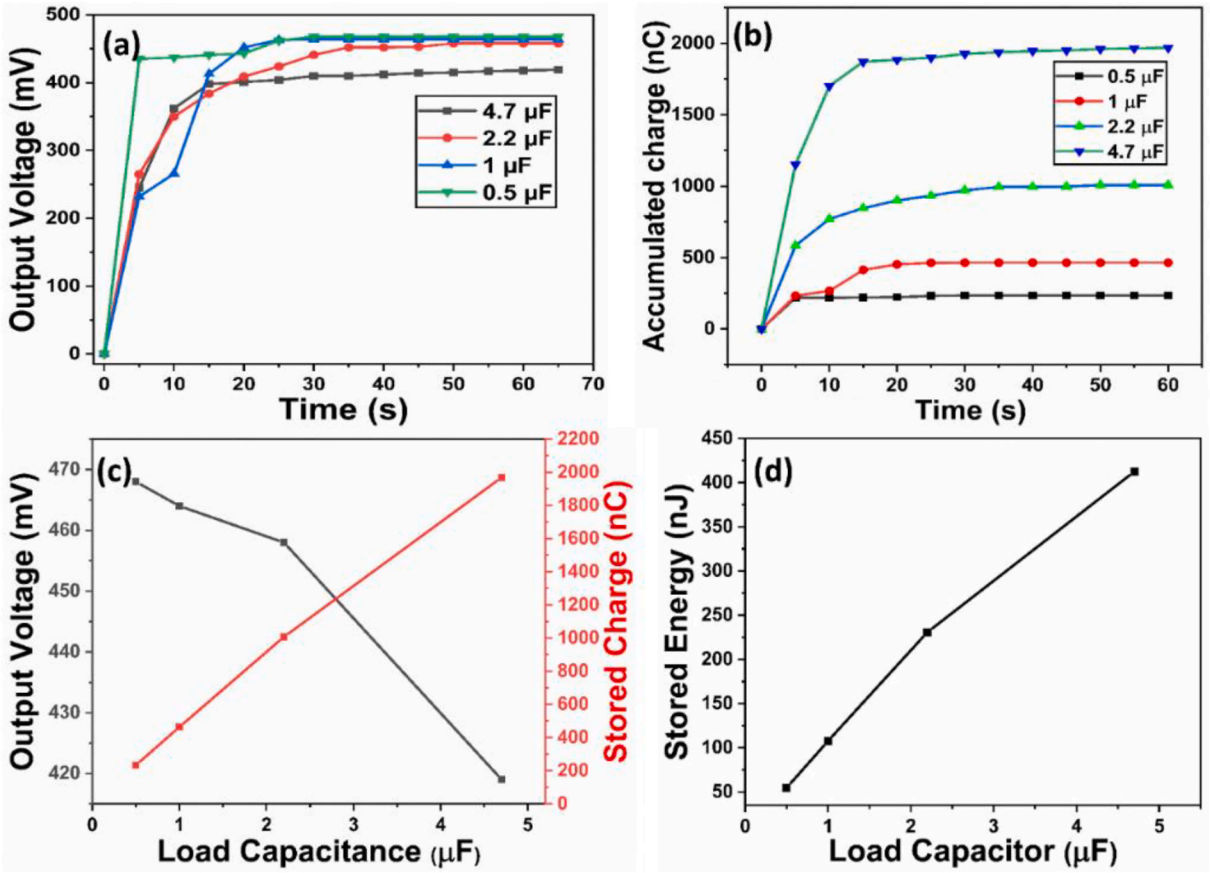

Fig. 5. **(a)** Output voltage across the capacitors, **(b)** Accumulated charge across the capacitors, **(c)** Highest output voltage across the capacitors and highest accumulated charge across all capacitors, **(d)** Maximum stored energy across load capacitors.

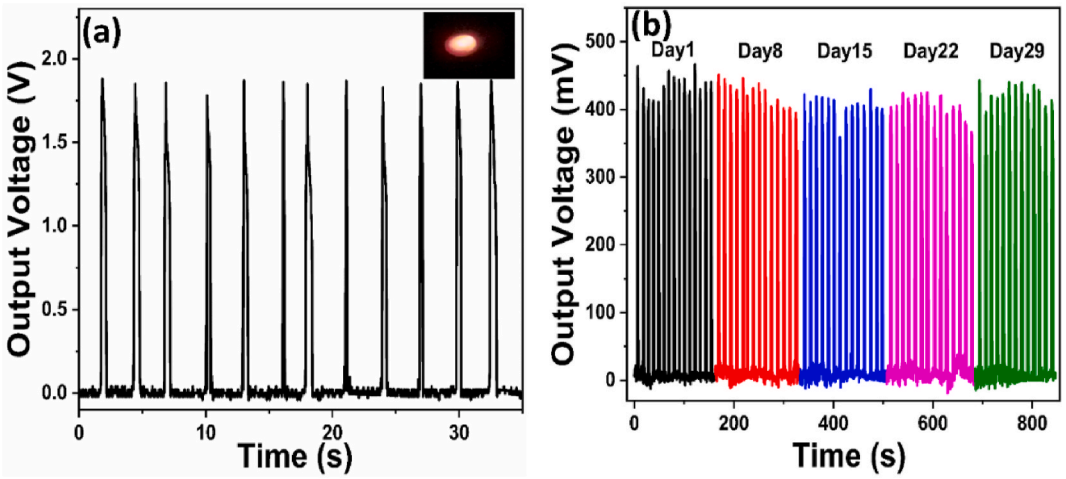

Fig. 6. **(a)** Output voltage of five devices in series (Glowing red LED in inset), **(b)** Repeatability of outcomes. (For interpretation of the references to colour in this figure legend, the reader is referred to the Web version of this article.)

The output voltage of five nanogenerator devices connected in series under forwarding bias conditions is shown in Fig. 6(a) and the inset figure is the real-time snap of a glowing commercial red LED across a 4.7 μF capacitor. The nanogenerator's repeatability was measured at different intervals of time, including immediately after manufacture, one week, two weeks, three weeks & four weeks respectively as shown in Fig. 6(b). In all circumstances, the nanogenerator produced roughly the same output voltage in response to mechanical stress exerted by the finger, which demonstrated the stability of the fabricated nanogenerator. Fig. 7 shows the fabricated nanogenerator response under various types of pressure created by punch, stick, toe, wrist movement respectively. The output voltage for punch (Fig. 7(a)) and toe pressure (Fig. 7(c)) was giving the highest voltage around 540 mV and 600 mV, respectively.

The major goal of our work is to extract energy from human movement. As a result, we used the stress caused by wrist movement to test the performance of our device for practical applications. We connect with CRO and fixed our device under the wrist. Scotch tape was used to

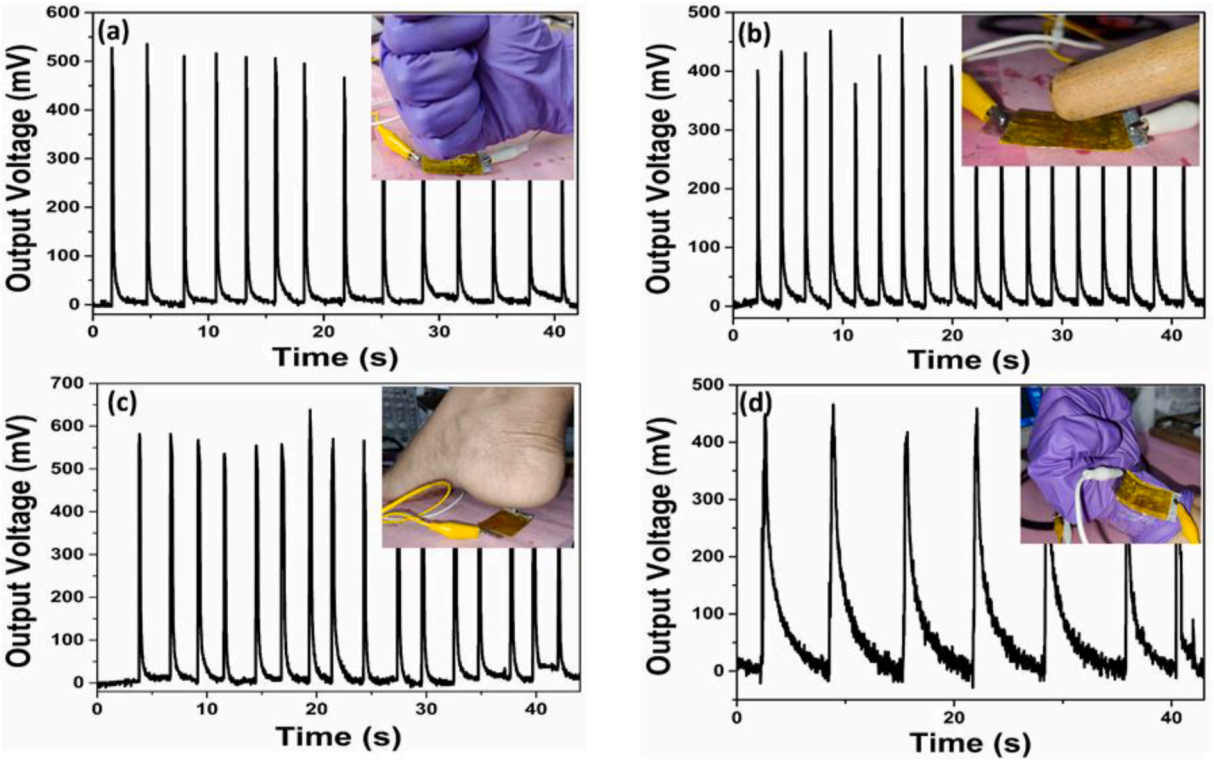

Fig. 7. (a) Output voltage due to punch, **(b)** Output voltage due to impact with a stick, **(c)** Highest output voltage with toe pressure, **(d)** Output voltage for wrist movement.

attach the nanogenerator device to the wrist, allowing it to encounter adequate strain when the wrist was folded. The inset of Fig. 7(d) shows the optical image of the nanogenerator in a folding state. The average voltage generated by this was about 450 mV as shown in Fig. 7(d). The outcome was verified to be reproducible by testing many nanogenerator devices (~20) developed under similar conditions (almost the same dimension). Further, a PENG was fabricated without zinc sulfide film (PENG0) and compared the power generation characteristics to our ZnS nanostructured based device. The output voltage response of the PENG with and without ZnS coating on aluminum substrate are shown in Fig. S2 of Supplementary Information. The output voltage of as-prepared PENG0 was tested against finger tapping as well as bending. Unfortunately, no output was observed due to short-circuit between two conducting plates i.e. Al and ITO-PET.

5. Conclusions

In conclusion, this research shows for the first time that ZnS nanosheets with a pure cubic structure have been prepared using modified low-temperature hydrothermal approach. The developed nanogenerator produced around 400 mV open-circuit voltage when finger tapped and around 600 mV with the toe. After switching polarity and voltage superposition measurements, the signals were confirmed to be coming from the nanogenerator device itself rather than instrumental noise. It could be understood that the output voltage generated in this study can be increased even higher by connecting more nanogenerators in series. This fabricated device was also tested for the real-time harvesting of biomechanical energies. The nanogenerator's remarkable stability and repeatability were confirmed at various time intervals and found to be extremely high.

CRediT authorship contribution statement

Siju Mishra: Data curation, Formal analysis, Investigation, Roles, Writing – original draft. **P. Supraja:** Data curation, Formal analysis, Investigation. **P.Ravi Sankar:** Formal analysis, Investigation. **R.Rakesh Kumar:** Conceptualization, Methodology, Supervision. **K. Prakash:** Data curation, Formal analysis. **D. Haranath:** Funding acquisition, Methodology, Supervision, Writing – review & editing.

Declaration of competing interest

The authors declare that they have no known competing financial interests or personal relationships that could have appeared to influence the work reported in this paper.

Acknowledgements

The authors are thankful to the sophisticated instrument centre, IIT Bhubaneswar, for the FE-SEM study. The authors acknowledge the Center for Advanced Materials (CAM), NIT Warangal for XRD, photoluminescence and UV-VIS spectroscopy studies.

Appendix A. Supplementary data

Supplementary data to this article can be found online at https://doi.org/10.1016/j.matchemphys.2021.125264.

References

[1] R. Singh, P.K. Singh, B. Bhattacharya, H.W. Rhee, Review of current progress in inorganic hole-transport materials for perovskite solar cells, Appl. Mater. Today. 14 (2019) 175–200, https://doi.org/10.1016/j.apmt.2018.12.011.
[2] Y. Hu, Z.L. Wang, Recent progress in piezoelectric nanogenerators as a sustainable power source in self-powered systems and active sensors, Nano Energy 14 (2014) 3–14, https://doi.org/10.1016/j.nanoen.2014.11.038.
[3] G. Zubi, R. Dufo-López, M. Carvalho, G. Pasaoglu, The lithium-ion battery: state of the art and future perspectives, Renew. Sustain. Energy Rev. 89 (2018) 292–308, https://doi.org/10.1016/j.rser.2018.03.002.
[4] O.H. Ando Junior, A.L.O. Maran, N.C. Henao, A review of the development and applications of thermoelectric microgenerators for energy harvesting, Renew.

Sustain. Energy Rev. 91 (2018) 376–393, https://doi.org/10.1016/j.rser.2018.03.052.
[5] Z. Lin, J. Song, Piezoelectric nanogenerators based on zinc oxide nanowire arrays author(s): zhong lin wang and jinhui song source, Science 312 (2006) 242–246, https://doi.org/10.1126/science.1124005, 80.
[6] B. Kumar, S. Kim, Energy harvesting based on semiconducting piezoelectric ZnO nanostructures, Nano Energy 1 (2012) 342–355, https://doi.org/10.1016/j.nanoen.2012.02.001.
[7] S. Xu, Z.L. Wang, One-dimensional ZnO nanostructures: solution growth and functional properties, Nano Res. 4 (2011) 1013–1098, https://doi.org/10.1007/s12274-011-0160-7.
[8] Z.L. Wang, Novel nanostructures of ZnO for nanoscale photonics, optoelectronics, piezoelectricity, and sensing, Appl. Phys. Mater. Sci. Process 88 (2007) 7–15, https://doi.org/10.1007/s00339-007-3942-8.
[9] X. Wang, J. Song, Z.L. Wang, Nanowire and nanobelt arrays of zinc oxide from synthesis to properties and to novel devices, J. Mater. Chem. 17 (2007) 711–720, https://doi.org/10.1039/b616963p.
[10] Z.L. Wang, Zinc oxide nanostructures: growth, properties and applications, J. Phys. Condens. Matter 16 (2004), https://doi.org/10.1088/0953-8984/16/25/R01.
[11] D. Barreca, D. Bekermann, A. Devi, R.A. Fischer, A. Gasparotto, C. MacCato, E. Tondello, M. Rossi, S. Orlanducci, M.L. Terranova, Novel insight into the alignment and structural ordering of supported ZnO nanorods, Chem. Phys. Lett. 500 (2010) 287–290, https://doi.org/10.1016/j.cplett.2010.10.030.
[12] D. Bekermann, A. Gasparotto, D. Barreca, L. Bovo, A. Devi, R.A. Fischer, O. I. Lebedev, C. MacCato, E. Tondello, G. Van Tendeloo, Highly oriented ZnO nanorod arrays by a novel plasma chemical vapor deposition process, Cryst. Growth Des. 10 (2010), https://doi.org/10.1021/cg1002012, 2011–2018.
[13] S.S. Mali, H. Kim, P.S. Patil, C.K. Hong, Chemically grown vertically aligned 1D ZnO nanorods with CdS coating for efficient quantum dot sensitized solar cells (QDSSC): a controlled synthesis route, Dalton Trans. 42 (2013) 16961–16967, https://doi.org/10.1039/c3dt51287h.
[14] B. Saravanakumar, S. Kim, Growth of 2D ZnO Nanowall for Energy Harvesting Application, 2014, https://doi.org/10.1021/jp502057p.
[15] D. Barreca, A. Gasparotto, C. Maccato, C. Maragno, E. Tondello, ZnO nanoplatelets obtained by chemical vapor deposition, studied by XPS, Surf. Sci. Spectra 14 (2007) 19–26, https://doi.org/10.1116/11.20071001.
[16] T. Wang, Y. Liu, G. Li, Z. Sun, J. Lu, B. Liu, M. Wu, Synthesis of highly-transparent Al-doped ZnO porous network thin films, CrystEngComm 13 (2011) 2661–2666, https://doi.org/10.1039/c0ce00890g.
[17] M.K. Gupta, J. Lee, K.Y. Lee, S. Kim, ZnO Nanosheet-Based Flexible Direct Current Nanogenerator, 2013, pp. 8932–8939, https://doi.org/10.1021/nn403428m.
[18] A. Umar, Y.B. Hahn, ZnO nanosheet networks and hexagonal nanodiscs grown on silicon substrate: growth mechanism and structural and optical properties, Nanotechnology 17 (2006) 2174–2180, https://doi.org/10.1088/0957-4484/17/9/016.
[19] R. Yang, Y. Qin, C. Li, L. Dai, Z.L. Wang, Characteristics of output voltage and current of integrated nanogenerators, Appl. Phys. Lett. 94 (2009) 92–95, https://doi.org/10.1063/1.3072362.
[20] S. Kar, A. Dev, S. Chaudhuri, Simple solvothermal route to synthesize ZnO nanosheets, nanonails, and well-aligned nanorod arrays, J. Phys. Chem. B 110 (2006) 17848–17853, https://doi.org/10.1021/jp0629902.
[21] S. Sahoo, S.K. Barik, A.P.S. Gaur, M. Correa, G. Singh, R.K. Katiyar, V.S. Puli, J. Liriano, R.S. Katiyar, Microwave assisted synthesis of ZnO nano-sheets and their application in UV-detector, ECS J. Solid State Sci. Technol. 1 (2012) Q140–Q143, https://doi.org/10.1149/2.023206jss.
[22] Y.C. Liang, C.S. Hung, W.C. Zhao, Thermal annealing induced controllable porosity and photoactive performance of 2d ZnO sheets, Nanomaterials 10 (2020) 1–15, https://doi.org/10.3390/nano10071352.
[23] P.T.H. Lai Van Duy, Nguyen Hong Hanh, Dang Ngoc Son, N.V.H. Chu Manh Hung, Nguyen Van Duy, Nguyen Duc Hoa, 2019, 10.1155@2019@4867909.Pdf, 2019.
[24] J.H. Park, Y.J. Choi, J.G. Park, Evolution of ZnO nanowires, nanorods, and nanosheets with an oxygen-assisted carbothermal reduction process, Mater. Res. Soc. Symp. Proc. 848 (2005) 415–420, https://doi.org/10.1557/proc-848-ff9.6.
[25] J. Yang, Y. Wang, J. Kong, H. Jia, Z. Wang, Synthesis of ZnO nanosheets via electrodeposition method and their optical properties, growth mechanism, Opt. Mater. 46 (2015) 179–185, https://doi.org/10.1016/j.optmat.2015.04.016.
[26] J.P. Cheng, Z.M. Liao, D. Shi, F. Liu, X.B. Zhang, Oriented ZnO nanoplates on Al substrate by solution growth technique, J. Alloys Compd. 480 (2009) 741–746, https://doi.org/10.1016/j.jallcom.2009.02.041.
[27] M.K. Gupta, J.H. Lee, K.Y. Lee, S.W. Kim, Two-dimensional vanadium-doped ZnO nanosheet-based flexible direct current nanogenerator, ACS Nano 7 (2013) 8932–8939, https://doi.org/10.1021/nn403428m.
[28] K.-H. Kim, B. Kumar, K.Y. Lee, H.-K. Park, J.-H. Lee, H.H. Lee, H. Jun, D. Lee, S.-W. Kim, Piezoelectric two-dimensional nanosheets/anionic layer heterojunction for efficient direct current power generation, Sci. Rep. 3 (2013) 2017, https://doi.org/10.1038/srep02017.
[29] H. Lee, H. Kim, D.Y. Kim, Y. Seo, Pure piezoelectricity generation by a flexible nanogenerator based on lead zirconate titanate nanofibers, ACS Omega 4 (2019) 2610–2617, https://doi.org/10.1021/acsomega.8b03325.
[30] K. Il Park, S. Xu, Y. Liu, G.T. Hwang, S.J.L. Kang, Z.L. Wang, K.J. Lee, Piezoelectric BaTiO3 thin film nanogenerator on plastic substrates, Nano Lett. 10 (2010) 4939–4943, https://doi.org/10.1021/nl102959k.
[31] L. Lin, C.-H. Lai, Y. Hu, Y. Zhang, X. Wang, C. Xu, R.L. Snyder, L.-J. Chen, Z. L. Wang, High output nanogenerator based on assembly of GaN nanowires, Nanotechnology 22 (2011), 475401, https://doi.org/10.1088/0957-4484/22/47/475401.
[32] G. Liu, S. Zhao, R.D.E. Henderson, Z. Leonenko, E. Abdel-Rahman, Z. Mi, D. Ban, Nanogenerators based on vertically aligned InN nanowires, Nanoscale 8 (2016) 2097–2106, https://doi.org/10.1039/c5nr06841j.
[33] Y.B. Lee, J.K. Han, S. Noothongkaew, S.K. Kim, W. Song, S. Myung, S.S. Lee, J. Lim, S.D. Bu, K.S. An, Toward arbitrary-direction energy harvesting through flexible piezoelectric nanogenerators using perovskite PbTiO3 nanotube Arrays, Adv. Mater. 29 (2017), https://doi.org/10.1002/adma.201604500.
[34] V. Khurana, R.R. Kisannagar, S.S. Domala, D. Gupta, In situ polarized ultrathin PVDF film-based flexible piezoelectric nanogenerators, ACS Appl. Electron. Mater. 2 (2020) 3409–3417, https://doi.org/10.1021/acsaelm.0c00667.
[35] A. Sultana, T.R. Middya, D. Mandal, ZnS-paper based flexible piezoelectric nanogenerator, AIP Conf. Proc. 1942 (2018), https://doi.org/10.1063/1.5029058.
[36] A. Sultana, M.M. Alam, S. Garain, T.K. Sinha, T.R. Middya, D. Mandal, An effective electrical throughput from PANI supplement ZnS nanorods and PDMS-based flexible piezoelectric nanogenerator for power up portable electronic devices: an alternative of MWCNT filler, ACS Appl. Mater. Interfaces 7 (2015), https://doi.org/10.1021/acsami.5b04669, 19091–19097.
[37] M.Y. Lu, J. Song, M.P. Lu, C.Y. Lee, L.J. Chen, Z.L. Wang, ZnO#ZnS heterojunction and ZnS nanowire arrays for electricity generation, ACS Nano 3 (2009) 357–362, https://doi.org/10.1021/nn800804r.
[38] H. Parangusan, J. Bhadra, N. Al-Thani, Flexible piezoelectric nanogenerator based on [P(VDF-HFP)]/PANI-ZnS electrospun nanofibers for electrical energy harvesting, J. Mater. Sci. Mater. Electron. 32 (2021) 6358–6368, https://doi.org/10.1007/s10854-021-05352-4.
[39] H. Parangusan, D. Ponnamma, M.A.A. Al-maadeed, Author correction : stretchable electrospun PVDF-HFP/Co- ZnO nanofibers as piezoelectric nanogenerators, Sci. Rep. (2018), 56281, https://doi.org/10.1038/s41598-019-56281-6.
[40] Y. Manjula, R. Rakesh Kumar, P.M. Swarup Raju, G. Anil Kumar, T. Venkatappa Rao, A. Akshaykranth, P. Supraja, Piezoelectric flexible nanogenerator based on ZnO nanosheet networks for mechanical energy harvesting, Chem. Phys. 533 (2020), 110699, https://doi.org/10.1016/j.chemphys.2020.110699.
[41] B. Yin, Y. Qiu, H. Zhang, J. Ji, L. Hu, Low-frequency flexible piezoelectric nanogenerators based on ZnO nanorods grown on Cu wires, CrystEngComm 16 (2014) 6831–6835, https://doi.org/10.1039/c4ce00954a.
[42] T.C. Hou, Y. Yang, Z.H. Lin, Y. Ding, C. Park, K.C. Pradel, L.J. Chen, Z. Lin Wang, Nanogenerator based on zinc blende CdTe micro/nanowires, Nano Energy 2 (2013) 387–393, https://doi.org/10.1016/j.nanoen.2012.11.004.
[43] S. Khan, J.S. Han, S.Y. Lee, S.H. Cho, ZnS nano-spheres formed by the aggregation of small crystallites and their photocatalytic degradation of eosin B, Chin. J. Chem. 35 (2017) 159–164, https://doi.org/10.1002/cjoc.201600725.
[44] V. Gaddam, R.R. Kumar, M. Parmar, G.R.K. Yaddanapudi, M.M. Nayak, K. Rajanna, Morphology controlled synthesis of Al doped ZnO nanosheets on Al alloy substrate by low-temperature solution growth method, RSC Adv. 5 (2015) 13519–13524, https://doi.org/10.1039/c4ra14049d.
[45] R.K. Chandrakar, R.N. Baghel, V.K. Chandra, B.P. Chandra, Synthesis, characterization and photoluminescence studies of undoped ZnS nanoparticles, Superlattice. Microst. 84 (2015) 132–143, https://doi.org/10.1016/j.spmi.2015.04.023.
[46] R. Ma, X. Wei, C. Wang, S. Mao, B. Chen, Y. Shao, Y. Fu, K. Yan, D. Peng, Reproducible mechanical-to-optical energy conversion in Mn (II) doped sphalerite ZnS, J. Lumin. 232 (2021), https://doi.org/10.1016/j.jlumin.2020.117838.
[47] D. Peng, Y. Jiang, B. Huang, Y. Du, J. Zhao, X. Zhang, R. Ma, S. Golovynskyi, B. Chen, F. Wang, A ZnS/CaZnOS heterojunction for efficient mechanical-to-optical energy conversion by conduction band offset, Adv. Mater. 32 (2020) 1–7, https://doi.org/10.1002/adma.201907747.
[48] F. Huo, Y. Wang, C. You, W. Deng, F. Yang, Y. Pu, Phase- and size-controllable synthesis with efficient photocatalytic activity of ZnS nanoparticles, J. Mater. Sci. 52 (2017) 5626–5633, https://doi.org/10.1007/s10853-017-0797-z.
[49] N. Shanmugam, S. Cholan, A. Sundaramanickam, G. Viruthagiri, N. Kannadasan, Temperature controlled synthesis of ZnS nanocrystals by simple chemical precipitation, Walailak J. Sci. Technol. 10 (2013) 149–157, https://doi.org/10.2004/wjst.v10i2.421.
[50] J. Liu, P. Fei, J. Song, X. Wang, C. Lao, R. Tummala, Z.L. Wang, Carrier density and Schottky barrier on the performance of DC nanogenerator, Nano Lett. 8 (2008) 328–332, https://doi.org/10.1021/nl0728470.
[51] M. Shekargoftar, R. Krumpolec, T. Homola, Enhancement of electrical properties of flexible ITO/PET by atmospheric pressure roll-to-roll plasma, Mater. Sci. Semicond. Process. 75 (2018) 95–102, https://doi.org/10.1016/j.mssp.2017.11.022.
[52] K.-H. Kim, B. Kumar, K.Y. Lee, H.-K. Park, J.-H. Lee, H.H. Lee, H. Jun, D. Lee, S.-W. Kim, Piezoelectric two-dimensional nanosheets/anionic layer heterojunction for efficient direct current power generation, Sci. Rep. 3 (2013) 2017, https://doi.org/10.1038/srep02017.
[53] Y. Manjula, R. Rakesh Kumar, P.M. Swarup Raju, G. Anil Kumar, T. Venkatappa Rao, A. Akshaykranth, P. Supraja, Piezoelectric flexible nanogenerator based on ZnO nanosheet networks for mechanical energy harvesting, Chem. Phys. 533 (2020), 110699, https://doi.org/10.1016/j.chemphys.2020.110699.
[54] S.A. Han, T.H. Kim, S.K. Kim, K.H. Lee, H.J. Park, J.H. Lee, S.W. Kim, Point-defect-passivated MoS2 nanosheet-based high performance piezoelectric nanogenerator, Adv. Mater. 30 (2018), https://doi.org/10.1002/adma.201800342.
[55] J.-H. Lee, J.Y. Park, E.B. Cho, T.Y. Kim, S.A. Han, T.-H. Kim, Y. Liu, S.K. Kim, C. J. Roh, H.-J. Yoon, H. Ryu, W. Seung, J.S. Lee, J. Lee, S.-W. Kim, Reliable piezoelectricity in bilayer WSe 2 for piezoelectric nanogenerators, Adv. Mater. 29 (2017), 1606667, https://doi.org/10.1002/adma.201606667.

[56] M. Lu, J. Song, M. Lu, C. Lee, L. Chen, Z.L. Wang, M. Lu, J. Song, M. Lu, C. Lee, L. Chen, Z.L. Wang, ZnO ⁷… ZnS Heterojunction and ZnS Generation, 3, 2009, pp. 357–362, https://doi.org/10.1021/nn800804r.
[57] B. Yin, Y. Qiu, H. Zhang, J. Lei, Y. Chang, J. Ji, Y. Luo, Y. Zhao, L. Hu, Piezoelectric performance enhancement of ZnO flexible nanogenerator by a NiO-ZnO p-n junction formation, Nano Energy 14 (2014) 95–101, https://doi.org/10.1016/j.nanoen.2015.01.032.
[58] S. Stassi, V. Cauda, C. Ottone, A. Chiodoni, C. Fabrizio, G. Canavese, Flexible piezoelectric energy nanogenerator based on ZnO nanotubes hosted in a polycarbonate membrane, Nano Energy 13 (2015) 474–481, https://doi.org/10.1016/j.nanoen.2015.03.024.
[59] A.K. Kasi Aminullah, B. Najma, J.K. Kasi, S. Rafique, M. Bokhari, Fabrication of piezoelectric nanogenerator using 3D-ZnO nanosheets and optimization of charge storage system, Mater. Res. Bull. 123 (2020), https://doi.org/10.1016/j.materresbull.2019.110711.